

Creep rupture curve for simultaneous creep deformation and degradation of geosynthetic reinforcement

W. Kongkitkul¹, F. Tatsuoka² and D. Hirakawa³

¹Postdoctoral Fellow, Department of Civil Engineering, Tokyo University of Science, 2641 Yamazaki, Noda, Chiba, 278-8510, Japan, Telephone: +81 4 7124 1501 (ext. 4074), Telefax: +81 4 7123 9766, E-mail: warat@rs.noda.tus.ac.jp

²Professor, Department of Civil Engineering, Tokyo University of Science, 2641 Yamazaki, Noda, Chiba, 278-8510, Japan, Telephone: +81 4 7122 9819, Telefax: +81 4 7123 9766, E-mail: tatsuoka@rs.noda.tus.ac.jp

³Assistant Professor, Department of Civil Engineering, Tokyo University of Science, 2641 Yamazaki, Noda, Chiba, 278-8510, Japan, Telephone: +81 4 7124 1501 (ext. 4074), Telefax: +81 4 7123 9766, E-mail: dhirakaw@rs.noda.tus.ac.jp

Received 19 June 2006, revised 13 February 2007, accepted 15 February 2007

ABSTRACT: The viscous property of polymer geosynthetic reinforcement, which causes creep deformation, is first summarised. The creep deformation and associated creep rupture characteristics, when subjected to long-term sustained loading under the following three conditions, are numerically simulated based on a non-linear three-component rheology model: (a) the load–strain behaviour is always free from material degradation; (b) the load–strain behaviour exhibits simultaneous viscous effects and material degradation as in usual actual field cases; and (c) the sustained loading starts after full material degradation has taken place. Case (c) is the one assumed in the currently most popular design method, in which the long-term tensile design strength is obtained by separately applying reduction factors for creep rupture and material degradation. This method underestimates the *true* creep rupture strength to an extent that depends on the viscous and material degradation properties of the geosynthetic reinforcement. In this paper a new method to obtain the design tensile strength is proposed, taking into account the new creep–rupture curve for simultaneous creep deformation and degradation.

KEYWORDS: Geosynthetics, Geogrid, Creep, Creep–rupture curve, Degradation, Viscous property, Ageing, Non-linear three-component model, Simulation

REFERENCE: Kongkitkul, W., Tatsuoka, F. & Hirakawa, D. (2007). Creep rupture curve for simultaneous creep deformation and degradation of geosynthetic reinforcement. *Geosynthetics International* 14, No. 4, 189–200 [doi: 10.1680/gein.2007.14.4.189]

1. INTRODUCTION

The use of polymer geosynthetic reinforcement has become popular in the construction of reinforced soil structures, often more than the use of metal strip/grid reinforcement. When metal reinforcement is used, the vertical and horizontal spacing are usually large, say 1 m, accounting for the relatively high resulting stiffness and strength. This arrangement results in less contact area with the backfill, which may result in a pullout failure (Lee *et al.* 1994). Another potential serious problem is the low bond stress when the reinforcement is placed in high water content clayey backfill. On the other hand, polymer geosynthetic reinforcement with a planar structure is placed in the backfill at a relatively small vertical spacing, say 30 cm, accounting for the relatively low stiffness and strength. As

a result, the deformation of polymer geosynthetic-reinforced soil (GRS) structures that takes place by the end of construction may become larger than that of metal-reinforced soil structures under otherwise the same conditions (e.g. Christopher *et al.* 1994). It is to be noted, however, that the deformation of reinforced soil structures at the end of construction, before service, is usually not a serious engineering problem unless it is too large. Rather, excessive residual deformation of structures due to viscous deformation of backfill and reinforcement that would take place while in service, long-term material degradation and the associated possibility of creep rupture of the reinforcement are potential serious problems. In this respect, the tensile deformation and strength properties of polymer geosynthetic reinforcement are known to be more or less viscous

taking into account the creep reduction factor (RF_{CR}) and the durability reduction factor (RF_D).

On the other hand, Allen and Bathurst (1996) and Greenwood (2002), among others, studied the uses of the creep reduction factor (RF_{CR}) and installation damage factor (RF_{ID}) when the effects of creep deformation and installation damage are separately taken into account and combined. They concluded that multiplication of creep reduction and installation damage factors (Figure 1) may also be conservative.

In view of the above, in the present study the viscous property of polymer geosynthetic reinforcement, which controls the creep strain and therefore the creep rupture strength, was first reviewed. Then the creep rupture strengths up to the end of the design life of typical civil engineering structures equal to 50 years were numerically simulated. This was done by introducing material degradation effects into a non-linear three-component rheology model (Figure 2; Tatsuoka *et al.* 2003; Di Benedetto *et al.* 2005) by extending the work of Tatsuoka *et al.* (2006). The three-component model was first developed to describe the rate dependence of the stress–strain behaviour of geomaterials (i.e. soils and rocks) not only in triaxial and plane-strain compressions but also in triaxial extension (Kiyota & Tatsuoka 2006). In the present study, the simulations of creep behaviour of geosynthetic reinforcement were performed for the following three cases:

- (1) when the material does not degrade at all during the design life;
- (2) when sustained loading (SL) starts after full material degradation for the service life has taken place and there is no degradation during SL (i.e. the case of Equation 1, which is illustrated in Figure 1); and
- (3) when material degradation takes place simultaneously during SL that continues over the design life (i.e. the actual case).

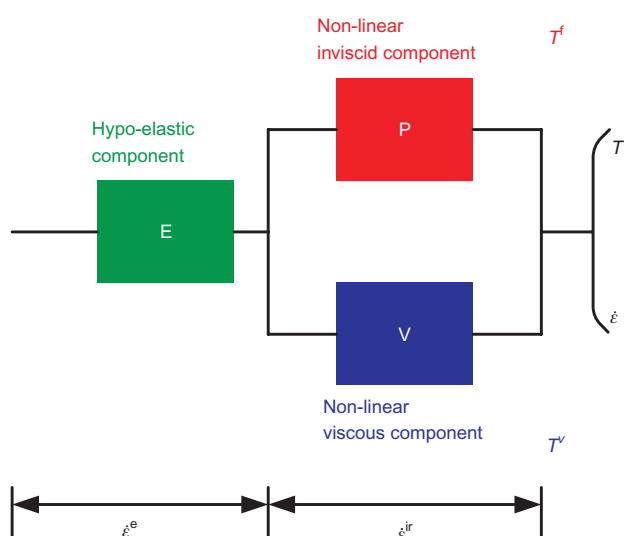


Figure 2. Non-linear three-component model for geosynthetic reinforcement (Hirakawa *et al.* 2003; Kongkitkul *et al.* 2004, 2007a, 2007b; Kongkitkul and Tatsuoka 2007)

Then, the creep rupture strengths for the three cases were compared. These simulations did not aim at analysis of the behaviour of any specific geosynthetic reinforcement type. Rather, the simulations were designed to represent the behaviour of typical geosynthetic reinforcement types. It is considered that the general trend of behaviour described in this paper is relevant to typical polymer geosynthetic reinforcement types used in practice.

2. VISCOUS PROPERTY OF POLYMER GEOSYNTHETIC REINFORCEMENT

A tensile load jump, ΔT , taking place upon a step increase or decrease in the strain rate, $\dot{\epsilon}$, applied during otherwise monotonic loading (ML) at a constant strain rate in a tensile loading test of a given geosynthetic reinforcement reflects its viscous properties (Figure 3). Unlike unbound geomaterials, most geosynthetic reinforcement types have isotach viscosity (Di Benedetto *et al.* 2002; Tatsuoka *et al.* 2002), for which, unless the loading direction is reversed with a change in the sign of irreversible strain rate, $\dot{\epsilon}^{ir}$, the current tensile load, T , is a unique function of instantaneous irreversible tensile strain, ϵ^{ir} , and $\dot{\epsilon}^{ir}$. Therefore ΔT upon a change in $\dot{\epsilon}^{ir}$ is persistent as long as $\dot{\epsilon}^{ir}$ is kept constant during the subsequent ML (e.g. Hirakawa *et al.* 2003; Kongkitkul *et al.* 2004, 2007a; Tatsuoka *et al.* 2006). The isotach property is described in more detail later in this paper.

The viscous property of a given geosynthetic reinforcement can be evaluated by plotting the normalised tensile load jump, $\Delta T/T$, where T is the instantaneous tensile load, against the logarithm of the ratio of $\dot{\epsilon}^{ir}$ values after and before a step change. Figure 4 shows this plot obtained from tensile tests on a number of polymer geogrids, a polyester (PET) yarn (i.e. a constituent of a geocomposite that bears the tensile load) and also the polypropylene (PP) filament (i.e. constituting fibre of PP geosynthetic, described below). The slope of a line fitted to the test

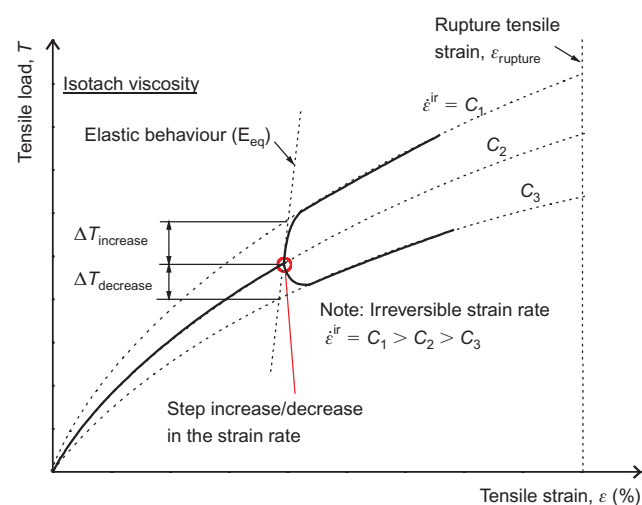


Figure 3. Quantification of viscous property of geosynthetic reinforcement from a tensile load jump upon a step increase/decrease in the strain rate

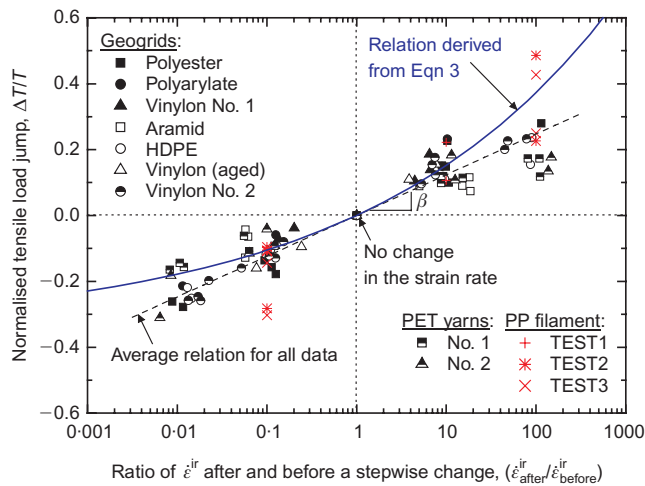


Figure 4. Rate sensitivity coefficients of geosynthetic reinforcement and polypropylene (PP) filament (after Hirakawa *et al.* 2003; Kongkitkul 2004)

result for a given material is defined as the rate-sensitivity coefficient, β (Tatsuoka 2004; Di Benedetto *et al.* 2005). The curve denoted by ‘relation derived from Equation 3’ in Figure 4 is explained later. The value of β and the rupture strengths from ML tests at $\dot{\epsilon} = 1.0\%/min$ of the tested materials are listed in Table 1. It may be seen that the range of these β values is relatively small. Moreover, the β value of Vinylon geogrids Nos. 1 and 2, with rupture strengths that differ by a factor of 2, which were provided by the same manufacturer, are very similar. This is also the case with the PET yarns Nos. 1 and 2, with rupture strengths differing by a factor of 3. This may be due to the fact that this pair of geosynthetic reinforcement products is made from the same raw material. On the other hand, the different numbers of filaments/textiles per yarn (i.e. different densities of filament) resulted in very different rupture strengths of the yarn.

The rate sensitivity coefficient, β , of different types of geosynthetic reinforcement was also obtained from the test results found in the literature (e.g. Figures 5a and 5b). Tensile loads, T , at the same strain rate, $\dot{\epsilon}$, were read from tensile load–tensile strain (T – ϵ) curves obtained from

Table 1. Rate sensitivity coefficients obtained by performing stepwise changes in the strain rate

No.	Reinforcement	β value	Rupture strength (kN/m) at $\dot{\epsilon} = 1.0\%/min$
1	Polyester	0.1428	39.2
2	Polyarylate	0.0732	88.0
3	Vinylon No. 1	0.1319	60.8
4	Aramid	0.0665	56.0
5	HDPE	0.1132	50.0
6	Vinylon (aged)	0.1595	59.0
7	PET yarn No. 1	0.0800	157.0
8	Vinylon No. 2	0.1345	33.3
9	PET yarn No. 2	0.0960	58.0
10	PP filament	0.1701	N/A

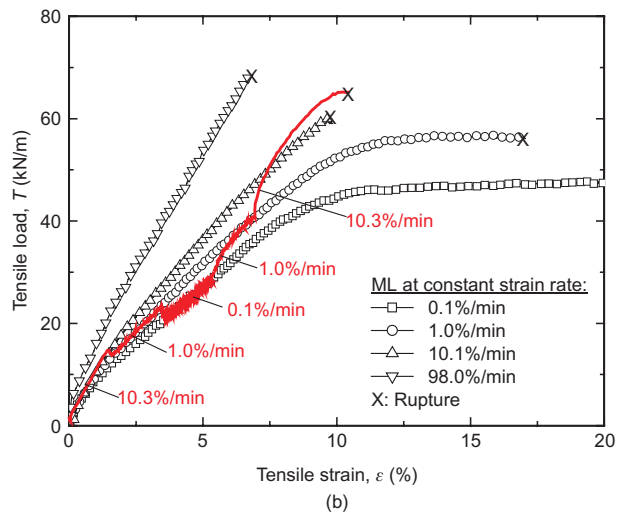
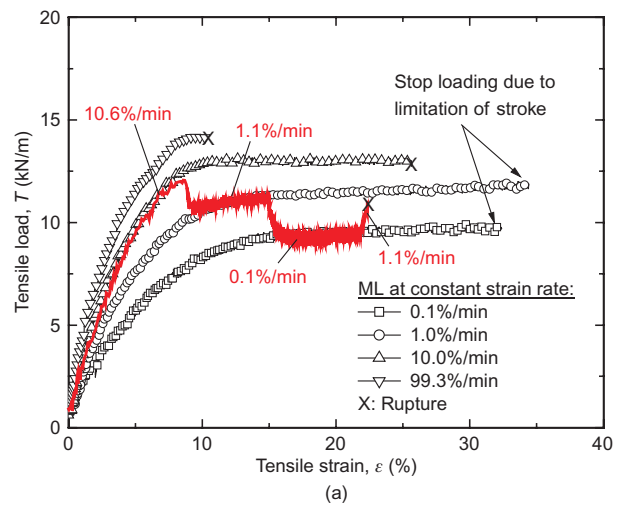


Figure 5. Rate-dependent T – ϵ relations of: (a) PP geogrid; (b) HDPE geogrid (after Shinoda and Bathurst 2004)

continuous ML tests at different strain rates. Assuming that the isotach viscosity is relevant, the difference in the tensile loads, ΔT , at the selected two different strain rates (e.g. C_1 and C_2 in Figure 3) for the same tensile strain was treated to be equivalent to the tensile load jump upon a strain rate change from C_2 to C_1 . Table 2 summarises these β values thus obtained, which are of the same order of magnitude as those listed in Table 1. It may be seen from Tables 1 and 2 that the β values of different products of the same geogrid type (i.e. HDPE) provided by different manufacturers are noticeably different.

Figure 6 shows the T – ϵ relations from a series of tensile tests on single polypropylene (PP) filaments in which the strain rate was stepwise changed during otherwise monotonic (ML) loading. In Figure 6, the tensile load has units of centi-newtons per single filament/textile. The trend of rate dependence seen in Figure 6 and the β value shown in Table 1 for PP filaments are similar to those of the PP geogrid (respectively in Figure 5a and Table 2). This result indicates that the viscous property of polymer geosynthetic reinforcement is basically controlled by the viscous property of the constituent material.

Table 2. Rate sensitivity coefficients derived from the literature

No.	Reinforcement	Range of $\dot{\epsilon}$ (%/min)	β value	Reference
1	HDPE	0.2 – 20 (0.2, 1, 10, 20)	0.2256	Hirai and Yatsu (2000)
2	HDPE	1 – 300 (1, 10, 60, 300)	0.3336	Bathurst and Cai (1994)
3	HDPE	0.1 – 98.1 (0.1, 1, 10.1, 98.1)	0.2524	Shinoda <i>et al.</i> (2002)
4	PET	1 – 125 (1, 10, 125)	0.1272	Bathurst and Cai (1994)
5	PP	0.1 – 99.3 (0.1, 1, 10, 99.3)	0.2326	Shinoda <i>et al.</i> (2002)
6	PP (Figure 5a)	Step changes in $\dot{\epsilon} = 0.1 - 10.6$	0.1837	Shinoda and Bathurst (2004)
7	HDPE (Figure 5b)	Step changes in $\dot{\epsilon} = 0.1 - 10.3$	0.1500	Shinoda and Bathurst (2004)

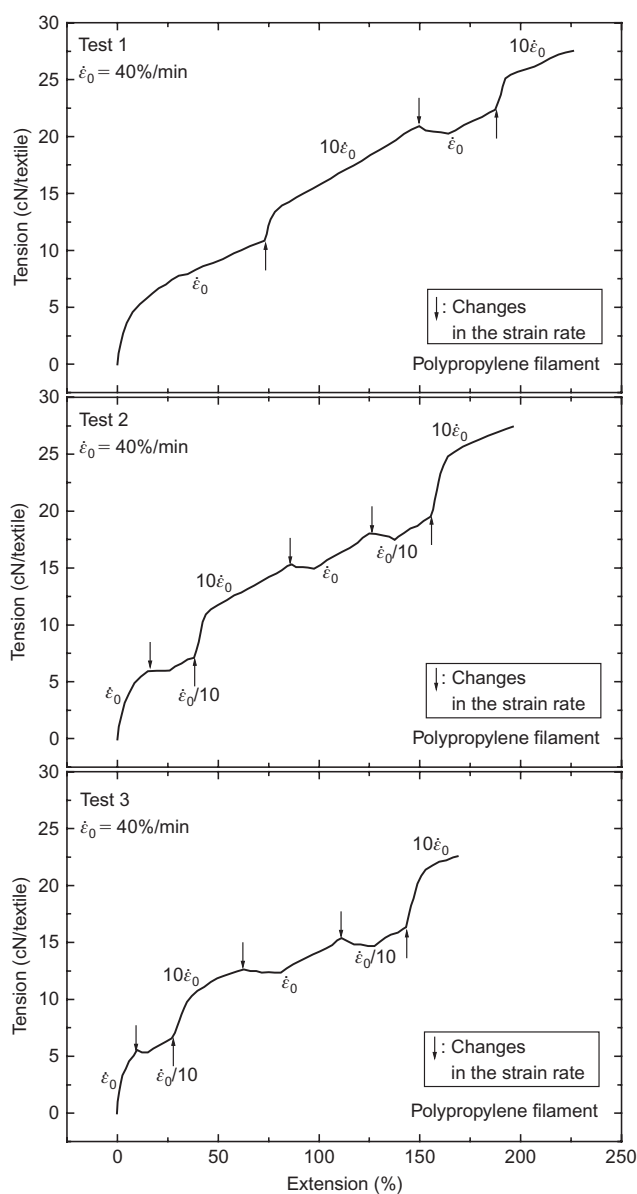


Figure 6. Rate-dependent $T-\epsilon$ relations of PP filament (after Kongkitkul 2004)

3. MODELLING OF VISCOUS PROPERTY AND MATERIAL DEGRADATION

3.1. General

A brief description of the non-linear three-component model (Figure 2) is given below. The details of the model

are described by Kongkitkul and Tatsuoka (2007). According to this model, the tensile load, T , is decomposed into the inviscid component, T^f , and the viscous component, T^v , representing the viscous property. The tensile strain rate, $\dot{\epsilon}$, is also decomposed into the elastic component, $\dot{\epsilon}^e$, and the irreversible (i.e. inelastic or viscoplastic) component, $\dot{\epsilon}^{ir}$. Elastic strain rates are obtained using a hypo-elastic model: $\dot{\epsilon}^e = \dot{T}/E_{eq}(T)$, where $E_{eq}(T)$ is the elastic stiffness, which is a function of the instantaneous tensile load, T . Tatsuoka *et al.* (2003) incorporated the ageing effects (positive and negative) into the non-linear three-component model (Figure 2) by introducing the yield inviscid stress that changes with time, t_c , having a specific origin. Then the inviscid component, T^f , during ML becomes dependent on t_c . By this modification, coupled simulations of ageing effects and elasto-viscoplastic behaviour of geomaterial became possible. Kongkitkul and Tatsuoka (2007) modified the model for this type of simulation applied to geosynthetic reinforcement.

3.2. Modelling for viscous properties

Most geosynthetic reinforcement types exhibit viscous properties of the isotach type (e.g. Hirakawa *et al.* 2003; Kongkitkul *et al.* 2004, 2007a; Shinoda and Bathurst 2004). For the case without ageing effects, the tensile load–strain ($T-\epsilon$) relation is always a unique function of the instantaneous irreversible strain and its rate. Subsequently, the isotach viscous component of tensile load, T_{iso}^v , is obtained as

$$T_{iso}^v = T^f(\epsilon^{ir}) \cdot g_v(\dot{\epsilon}^{ir}) \tag{2}$$

where $g_v(\dot{\epsilon}^{ir})$ is the viscosity function (i.e. a non-linear function of $\dot{\epsilon}^{ir}$). In the present study, the following non-linear function proposed for geomaterial (Di Benedetto *et al.* 1999) was used:

$$g_v(\dot{\epsilon}^{ir}) = \alpha^* \cdot (\dot{\epsilon}^{ir}/\dot{\epsilon}_0^{ir})^{1+b^*} \tag{3}$$

where α^* , b^* and $\dot{\epsilon}_0^{ir}$ are material constants. The parameters $\alpha^* = 0.36$, $1 + b^* = 0.16$ and $\dot{\epsilon}_0^{ir} = 10^{-3}\%/s$ were selected in order to provide an average relevant range of viscous response upon a step increase or decrease in the tensile strain rate (Figure 4). That is, Equation 3 with these parameters is expressed by a non-linear relation in Figure 4. It may be seen that this relation is representative of the viscous property of these polymer geosynthetic reinforcement types. Equation 3 was used because creep

strain rates during sustained loading for a period of 50 years that are to be analysed become very low at late stages, and Equation 3 is much more relevant to this type of very long-term creep analysis than the expression previously used to analyse the creep strains for shorter periods (i.e. up to 30 days; Kongkitkul *et al.* 2007a).

3.3. Modelling for degradations

There are two types of ageing effect: the first one is positive, such as cementation effects for geomaterials, while the other one is negative, such as material degradation of polymer geosynthetic reinforcement by chemical or biological attacks. The latter effect is taken into account by introducing the durability reduction factor RF_D in Equation 1 in the design of GRS structures. In the numerical simulations in the present study, the negative ageing effects were taken into account as described below.

With ageing effects, the current inviscid tensile load, $[T^f]_{(\varepsilon^{ir}, t_c)}$, becomes a function not only of current irreversible strain, ε^{ir} , but also of the current time, t_c (having a fixed origin defined at the start of ageing, not the general time), and is obtained from

$$[T^f]_{(\varepsilon^{ir}, t_c)} = \int_{\tau=\varepsilon_1^{ir}, t=t_{c1}}^{\varepsilon^{ir}, t_c} [dT^f]_{(\tau, t)} \quad (4)$$

where $[dT^f]_{(\tau, t)}$ is the inviscid tensile load increment that develops when the ageing time is t and the irreversible strain is equal to τ ; and ε_1^{ir} and t_{c1} are the irreversible strain ε^{ir} and the ageing time at the start of loading with a fixed origin where $T^f = 0$.

Yielding of the inviscid load T^f associated with the development of positive irreversible strain increment ($d\varepsilon^{ir} > 0$) takes place when the following conditions are satisfied:

$$[T^f]_{(\tau, t)} = [T_y^f]_{(\tau, t)} \quad \text{and} \quad [dT^f]_{(\tau, t)} = [dT_y^f]_{(\tau, t)} \quad (5)$$

where T_y^f is the yield inviscid load that is subjected to ageing effects. The yield inviscid load increment, $[dT_y^f]_{(\tau, t)}$, for a given step of loading from the moment when $\varepsilon^{ir} = \tau$ and $t_c = t$ to the moment when $\varepsilon^{ir} = \tau + d\tau$ and $t_c = t + dt$ consists of the following two components (Figure 7 and Equation 6):

- a component that changes by $d\tau$ for $dt = 0$, $[E^f(\tau, t)]_{(dt=0)} \cdot d\tau$; and
- the other component that changes by dt for $d\tau = 0$, $[F^f(\tau, t)]_{(d\tau=0)} \cdot dt$.

$$[dT_y^f]_{(\tau, t)} = [E^f(\tau, t)]_{(dt=0)} \cdot d\tau + [F^f(\tau, t)]_{(d\tau=0)} \cdot dt \quad (6)$$

For a given value of dt , $[dT_y^f]_{(\tau, t)}$ has a non-zero positive value for positive ageing effects and a non-zero negative value for negative ageing effects, even under non-yielding conditions. When T_y^f is assumed to be independent of loading history (Tatsuoka *et al.* 2003; Kongkitkul and Tatsuoka 2007), Equation 6 becomes the following totally differentiable equation:

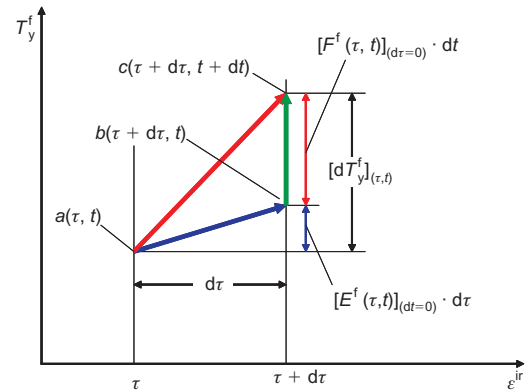


Figure 7. Yield inviscid tensile load increment by increments of irreversible strain and time (Tatsuoka *et al.* 2003; Kongkitkul and Tatsuoka 2007)

$$[dT_y^f]_{(\tau, t)} = \left[\frac{dT_0^f(\tau)}{d\tau} \cdot A^f(t) \right] \cdot d\tau + \left[T_0^f(\tau) \cdot \frac{dA^f(t)}{dt} \right] \cdot dt \quad (7)$$

By integrating Equation 7, we obtain the following loading history-independent equation:

$$[T_y^f]_{(\varepsilon^{ir}, t_c)} = T_y^f(\varepsilon^{ir}, t_c) = T_0^f(\varepsilon^{ir}) \cdot A^f(t_c) \quad (8)$$

where $T_0^f(\varepsilon^{ir})$ is the basic inviscid tensile load component, independent of any ageing effects. Equation 8 assumes that, when ageing effects are negative, T_y^f at a given ε^{ir} decreases by a factor of $A^f(t_c)$ with an increase in the elapsed time t_c since the start of material degradation (Figure 8).

4. SIMULATIONS

The T - ε relations were simulated for a loading history where monotonic loading (ML) at the same strain rate (1.0%/min) starts from $T = 0$ and continues until the start of 50-year sustained loading (SL) at different levels of

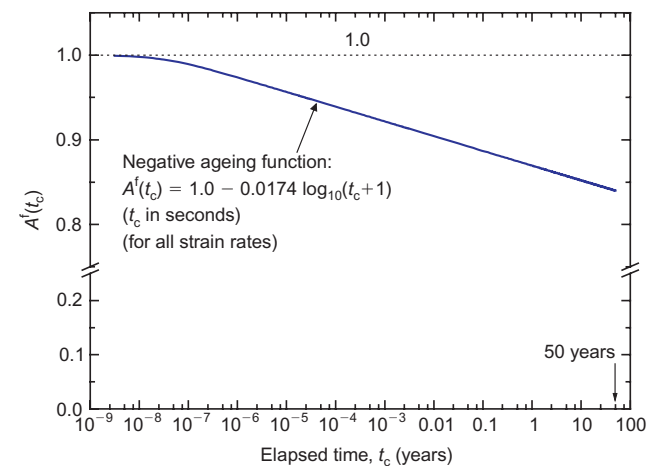


Figure 8. Negative ageing function assumed in the simulation

tensile load. The following three different patterns of material degradation were analysed:

Case 1 The $T-\epsilon$ property does not degrade with time at any moment. The results of simulation are presented in Figure 9a.

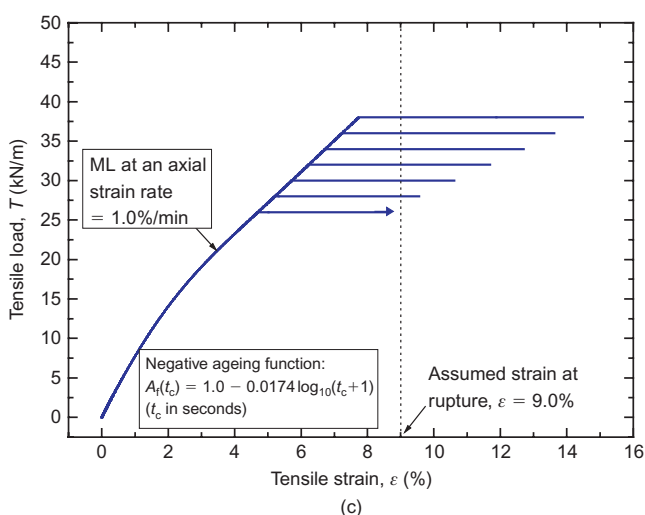
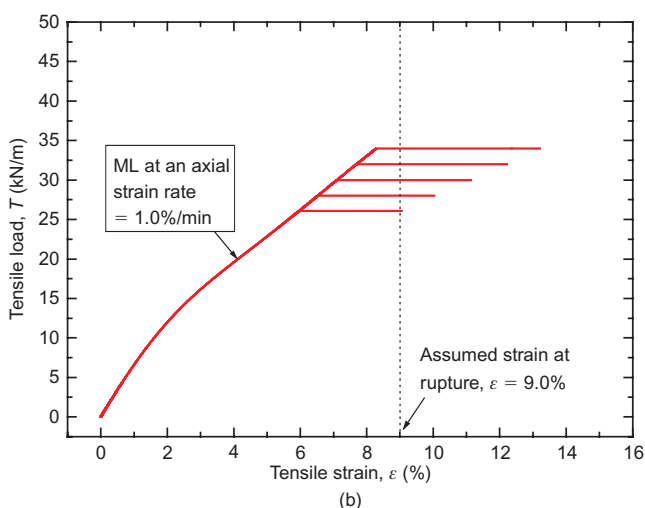
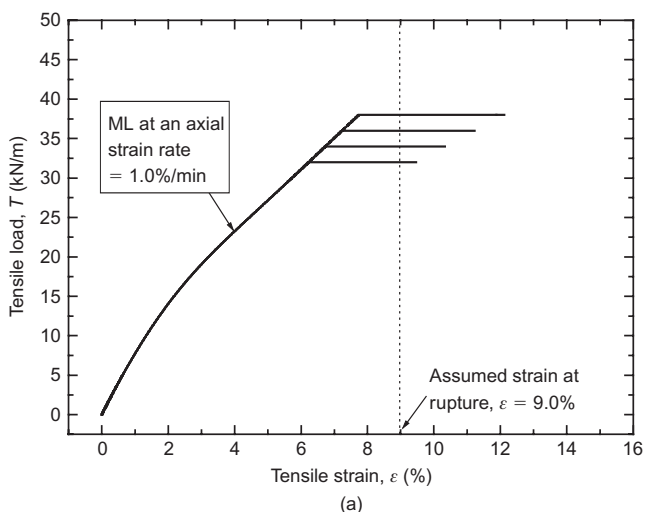


Figure 9. Simulated $T-\epsilon$ relations by ML at $\dot{\epsilon} = 1.0\%/min$ followed by SL stages: (a) case 1, no degradation; (b) case 2, SL after full degradation for 50 years; (c) case 3, degradation during SL

Case 2 ML starts after the $T-\epsilon$ property has degraded while T has been kept equal to 0 (i.e. zero tensile load) for full service life (i.e. 50 years in the present case). Then, no material degradation takes place after the start of ML, during which subsequently 50-year SL starts. That is, degradation has taken place only for a period of 50 years without any tensile load and the degradation has completely stopped before the start of ML. This is the case that is assumed in current design methods (Equation 1 and Figure 1). The results of simulation are presented in Figure 9b.

Case 3 Material degradation starts at the start of 50-year SL and subsequently continues during the SL. This is the actual case. The results of simulation are presented in Figure 9c. In this case, the effects of material degradation during ML until the start of SL, if taken into account, are negligible.

In case 2, it is assumed that the following negative time-dependent degradation function $A^f(t_c)$ (Figure 8) is effective only while the geosynthetic reinforcement is left without tensile load over its design life:

$$A^f(t_c) = 1.0 - 0.0174 \log_{10}(t_c + 1) \quad (9)$$

where t_c is the time increment in seconds since the start of material degradation (i.e. at the start of loading for the design life time). It is likely that the degradation function, $A^f(t_c)$, may be different for different geosynthetics types. Although Equation 9 was rather arbitrarily assumed, it was inevitable because no relevant experimental data are reported in the literature, to the best of the writers' knowledge. Despite the above, the conclusions from this study do not change with the use of another function for $A^f(t_c)$ that continuously decreases from 1.0 to a lower positive value with time, t_c .

In case 3, it is assumed that A^f is kept equal to 1.0 during monotonic loading (ML) from $T = 0$ until the start of respective sustained loading (SL) and then Equation 9 is made effective, where $t_c = 0$ at the start of the respective SL stage.

Figures 10a and 10b compare the simulated $T-\epsilon$ relations when SL for 50 years starts at, respectively, $T = 32$ kN/m and $T = 34$ kN/m during otherwise ML for cases 1, 2 and 3. Note that the $T-\epsilon$ relations during ML before the start of SL for cases 1 and 3 are exactly the same, as material degradation begins at the start of SL in case 3. Similar comparisons of the time history of tensile strain are presented in Figures 11a and 11b. Moreover, Figures 12a and 12b show the creep strains when $T = 32$ kN/m and $T = 34$ kN/m, respectively, plotted against the elapsed time (logarithmic scale) since the start of respective SL. It may be seen that the creep strain at the end of service life in case 3 (the assumed actual behaviour) is much larger than that in case 1 owing to continuous degradation during SL in case 3. On the other hand, the creep strain in case 3 is consistently smaller than that in case 2 (i.e. the current design method). Consequently, the creep strain for the same elapsed time since the start of SL in case 3 is always

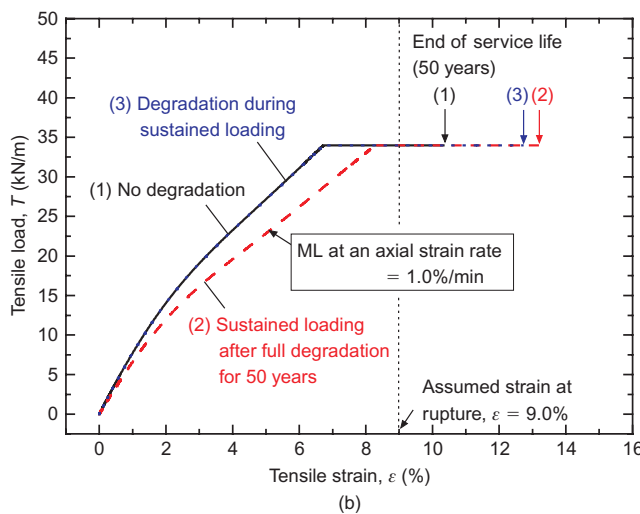
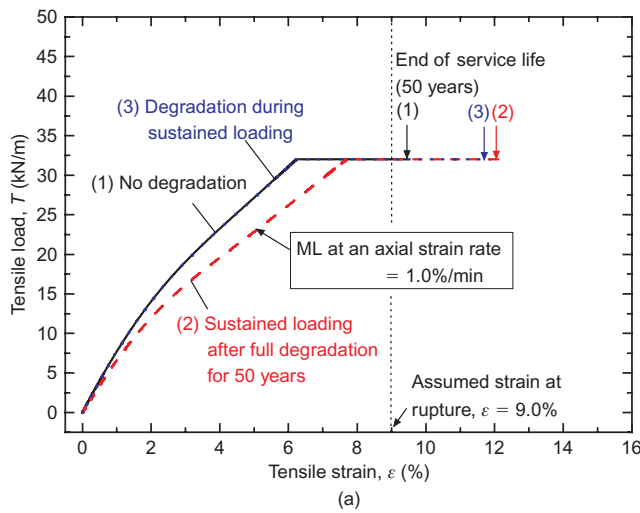


Figure 10. Comparison of T - ϵ relations under three different degradation conditions for SL stages at: (a) $T = 32$ kN/m; (b) $T = 34$ kN/m

between values for cases 1 and 2 until the end of service life.

5. CREEP RUPTURE CURVES

With an increase in the ambient temperature under otherwise the same conditions, for a given polymer geosynthetic reinforcement, the ultimate strength decreases while the strain at ultimate state increases and the stiffness or modulus of tensile load-strain relation substantially decreases (e.g. Zornberg and Kavazanjian 2002; Zornberg *et al.* 2004). On the other hand, Hirakawa *et al.* (2003) reported that, for all the geosynthetic reinforcement types tested in a comprehensive series of tensile loading tests on a number of geosynthetic reinforcement types at essentially the same controlled environment (i.e. at the same temperature and humidity), the strain at tensile rupture of each type of geosynthetic reinforcement was nearly the same irrespective of applied different pre-rupture loading histories and loading periods until rupture as well as largely different strain rates at rupture. In this study, it was assumed that the rupture tensile strain (i.e. the tensile strain at rupture in Figures 9a, 9b and 9c) is equal to

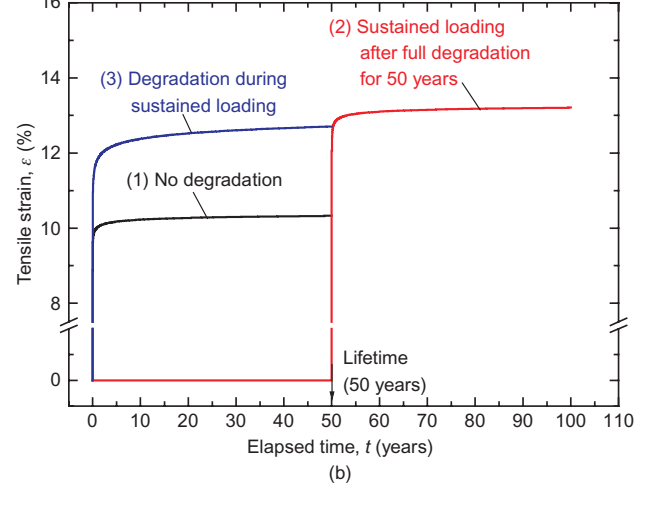
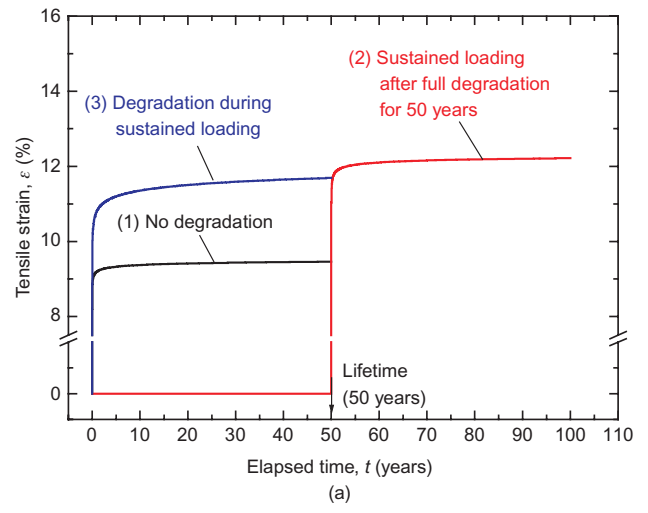


Figure 11. Time histories of tensile strain under three different degradation conditions for SL stages at: (a) $T = 32$ kN/m; (b) $T = 34$ kN/m

9.0%, irrespective of histories of loading and material degradation as well as strain rate. Note that the conclusions from the present study do not change by using other rupture strains. Kongkitkul and Tatsuoka (2007) employed the same assumption with respect to the rupture tensile strain to obtain the creep rupture curves from a set of master curves that were obtained from direct simulation of 50-year SL, numerical time-temperature superposition (TTS) tests and stepped isothermal method (SIM) tests.

As indicated in Figures 12a and 12b, the elapsed time when the creep rupture takes place (i.e. when the total strain, ϵ , defined as zero at the start of ML, becomes 9.0%) during the respective SL, since its start can be derived for the three different cases of degradation. In this way, the relationships between the sustained load and the corresponding creep rupture time since the start of SL (i.e. the creep rupture curves) were obtained for the three different cases of material degradation, as shown in Figure 13. The following trends of behaviour may be seen from Figure 13.

- (1) The creep rupture strength in case 3 (the assumed actual case) is smaller than that in case 1 (no

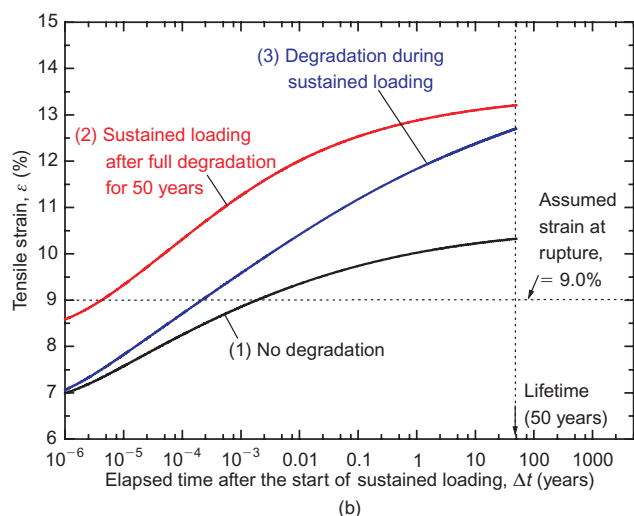
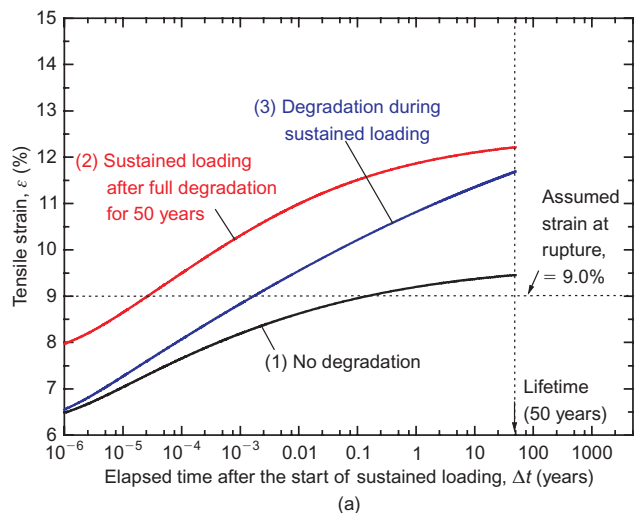


Figure 12. Relationship between tensile strain and elapsed time (in log-scale) since the start of SL stage under three different degradation conditions: (a) $T = 32$ kN/m; (b) $T = 34$ kN/m

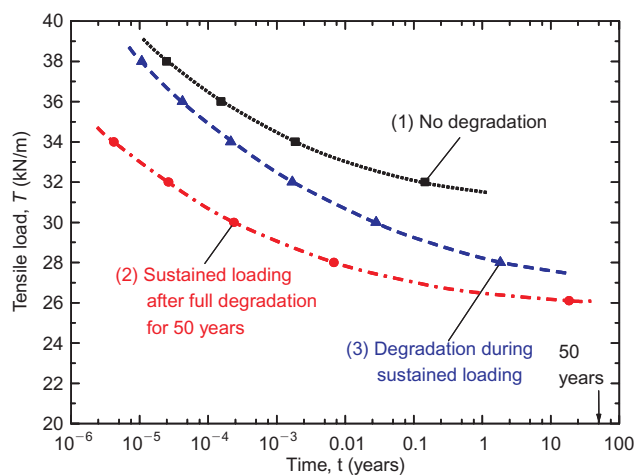


Figure 13. Creep rupture curves obtained by simulation under three different degradation conditions

material degradation), and the difference increases with an increase in the elapsed time.

- (2) On the other hand, the creep rupture strength in case 2 (the current design method) is consistently smaller

- than that in case 1. The difference is fairly constant for the full range of elapsed time examined.
- (3) A noticeable difference between the creep rupture strengths in cases 2 and 3 remains, even at the end of service life (50 years). Note that, owing to the logarithmic scale used for time in this figure, a small difference in the creep rupture strength results in a significant increase in the time until creep rupture for a given tensile load. It seems therefore that the design strength of a given geosynthetic reinforcement determined by Equation 1 based on the creep rupture curve in case 2 more or less underestimates the actual creep rupture strength at the end of service life.

A new creep rupture curve when material degradation takes place simultaneously with creep strain during sustained loading is schematically illustrated in a diagram presenting a newly proposed method to obtain the design strength (Figure 14). This new creep rupture curve starts from the tensile load before material degradation obtained at the time of construction of a given geosynthetic-reinforced soil (GRS) structure. At the end of service life, the tensile creep rupture strength obtained from this new creep rupture curve is higher than the value that is obtained by the current method (Equation 1) based on the conventional creep rupture curve (case 2 in Figure 13). This result suggests that, even when the overall safety factor was equal to unity (which is never employed in engineering practice), the current design method (Equation 1) is more conservative than it should be: that is, even when the design tensile rupture strength, T_d , is determined based on Equation 1, we can use a creep reduction factor, RF_{CR} , that is smaller than those used in the current practice. In actuality, with the use of an overall safety factor, the likely working long-term sustained load can be expected to be much lower than the creep rupture strength, whether determined based on the conventional creep rupture curve or on the new creep rupture curve. Furthermore, recent studies (Kongkitkul *et al.* 2007b) have shown that it is very likely that the tensile load activated in the polymer geosynthetic reinforcement used in conventional GRS structures at long-term working load may decrease with time owing to a type of stress relaxation phenomenon related to the interaction effects of the viscous properties of the backfill and reinforcement.

Tatsuoka *et al.* (2004) proposed to eliminate the creep reduction factor, RF_{CR} , from Equation 1. The following steps 1 to 5, illustrated in Figure 14, describe this method, which has been modified by introducing the new creep rupture curve obtained from the present study.

- (1) The ultimate strength, T_{ult} , of a given geosynthetic reinforcement at a given design strain rate, which is equal to the value at failure of a given GRS, is determined by relevant tensile loading tests. Different design strain rates at failure under static and seismic loading conditions should be defined. For example, the strain rate at rupture under seismic

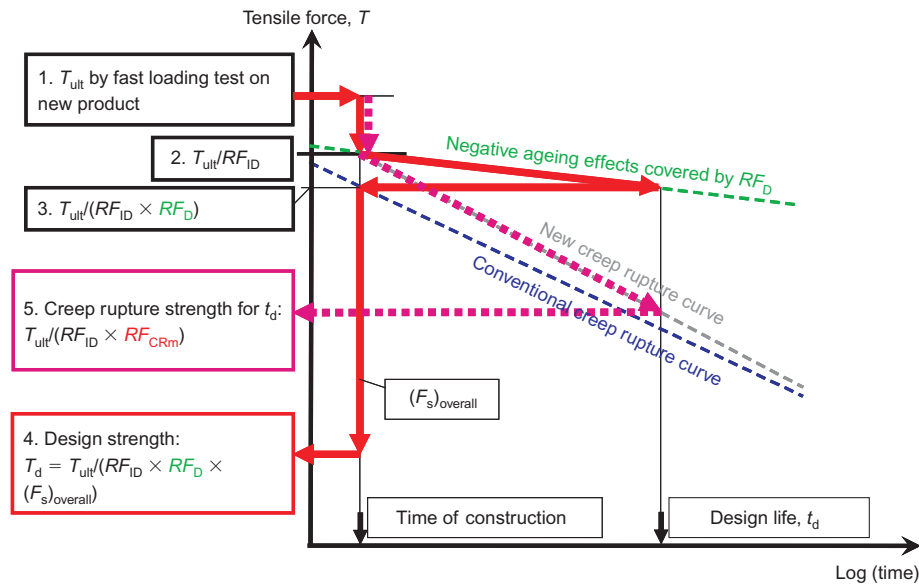


Figure 14. New proposed method to obtain the design strength (not controlled by creep rupture) of a geosynthetic reinforcement

- loading conditions may be greater by a factor of 1000 than the value under static loading conditions.
- (2) The value of T_{ult} obtained from step 1 is reduced by a factor of RF_{ID} accounting for installation damage (in the same way as Equation 1).
 - (3) RF_D to account for the chemical and/or biological degradation is estimated for the design life. Then the value of T_{ult}/RF_{ID} is reduced by a factor of estimated RF_D (in the same way as in Equation 1).
 - (4) It is confirmed that the ultimate tensile strength under static and seismic loading conditions, $(T_{ult})_{static}$ and $(T_{ult})_{seismic}$, that have been determined at step (1) satisfy the following two conditions:

$$(T_d)_{static} = \frac{(T_{ult})_{static}}{RF_D \cdot RF_{ID} \cdot (F_s)_{overall,static}} \quad (10a)$$

$$(T_d)_{seismic} = \frac{(T_{ult})_{seismic}}{RF_D \cdot RF_{ID} \cdot (F_s)_{overall,seismic}} \quad (10b)$$

$(T_d)_{static}$ and $(T_d)_{seismic}$ are the design static and seismic working loads, which are obtained by relevant stability analysis with $(F_s)_{overall} = 1.0$. It is suggested that the residual angle of friction be used as the design shear strength of backfill for static loading conditions to be conservative for design. For seismic loading conditions, it is suggested that the peak shear strength be used to locate critical failure planes, while the limit equilibrium along the located critical failure planes is evaluated by using the residual shear strength. This method was proposed by Tatsuoka *et al.* (1998) for the seismic design of GRS retaining walls, referring to the seismic design method for retaining walls with unreinforced backfill (Koseki *et al.* 1998). Leshchinsky (2001) also used this approach for selection of soil strength values for limit-equilibrium-based stability analysis of reinforced soil structures. Then, convert the value of $(T_{ult})_{seismic}$ to the value at the strain rate at which

$(T_{ult})_{static}$ is obtained, $(T_{ult})_{seismic}^*$. Next, the larger value of $(T_{ult})_{static}$ (Equation 10a) and $(T_{ult})_{seismic}^*$ is chosen as the ultimate tensile strength, T_{ult} , of a given geosynthetic reinforcement type, which is used in step (5).

- (5) It is confirmed that the design static load, $(T_d)_{static}$, is smaller than the creep rupture strength, $T_{ult}/(RF_{ID} \cdot RF_{CR,m})$, which is obtained based on the new creep rupture curve (Figure 14). Here, $RF_{CR,m}$ is the modified creep reduction factor, which includes the effects of simultaneous material degradation and creep deformation (case 3). The new creep rupture curve for a given type of polymer geosynthetic reinforcement can be obtained by numerical simulation for given conditions of simultaneous creep deformation and degradation, as performed in the present study. According to the worked examples reported by Tatsuoka *et al.* (2004), this requirement is usually easily satisfied.

It is considered that this newly proposed design method is relevant in particular when seismic design is important. That is, when seismic design is introduced, $(T_d)_{seismic}$ tends to become larger than $(T_d)_{static}$, and also $(T_{ult})_{seismic}^*$ tends to become larger than $(T_{ult})_{static}$. Therefore the creep rupture strength is determined by $(T_{ult})_{seismic}^*/(RF_{ID} \cdot RF_{CR,m})$. Then, it becomes likely that the long-term static working load, $(T_d)_{static}$, becomes sufficiently smaller than the creep rupture strength, $(T_{ult})_{seismic}^*/(RF_{ID} \cdot RF_{CR,m})$.

6. CONCLUSIONS

In current design methods to obtain the long-term design strength of geosynthetic reinforcement, the effects of creep deformation and material degradation on the possibility of creep rupture are *separately* taken into account. That is,

current design methods assume that sustained loading starts after the full material degradation for a given design life has taken place. However, the two mechanisms are simultaneously active during a given design life in actual cases. A series of numerical simulations was performed based on a non-linear three-component model taking into account ageing effects. The simulations showed that, at the end of a given design life, the creep rupture strength, when creep deformation and material degradation take place simultaneously during a given design life, becomes larger than the value obtained by following the current design methods. Therefore the current design methods underestimate the *true* creep rupture strength. Finally, it is suggested that the long-term design tensile strength be determined without using a creep reduction factor while confirming that the design strength is smaller than the creep rupture strength determined based on the new creep rupture strength. The new creep rupture strength can be determined by relevant numerical analysis in which creep deformation and material degradation take place simultaneously during a given design lifetime, as shown in this paper.

ACKNOWLEDGEMENTS

This study was supported by the Japan Society for the Promotion of Science through the grant 'Advanced application of soil reinforcement technology to highly earthquake-resistant reinforcement of existing soil structures and construction of highly earthquake-resistant and environment-friendly soil structures'. The writers are also grateful to G. Mannsbart, Polyfelt GmbH, Austria, for permission to use the data for the PP filaments reported in the paper.

NOTATIONS

Basic SI units are given in parentheses.

A^f	ageing function (dimensionless)
g_v	viscosity function of non-linear three-component model (dimensionless)
b^*	parameter of viscosity function (dimensionless)
$(F_s)_{\text{overall}}$	overall factor of safety to account for uncertainties in geometry of structure, fill properties, and external applied loads (dimensionless)
RF_{CR}	creep reduction factor (dimensionless)
$RF_{CR,m}$	modified creep reduction factor (dimensionless)
RF_D	durability reduction factor (dimensionless)
RF_{ID}	installation damage factor (dimensionless)
T	tensile load (N/m)
ΔT	tensile load increment (N/m)
T_d	design tensile strength (N/m)
T^f	inviscid tensile load of non-linear three-component model (N/m)
dT^f	inviscid tensile load increment used in integration for given step of loading (N/m)

T_y^f	yield inviscid tensile load of non-linear three-component model (N/m)
T_0^f	basic inviscid tensile load that is independent of any ageing effects (N/m)
dT_y^f	yield inviscid tensile load increment used in integration for given step of loading (N/m)
T_{ult}	ultimate tensile strength based on minimum average roll value (N/m)
T^v	viscous tensile load of non-linear three-component model (N/m)
T_{iso}^v	viscous tensile load of isotach type (N/m)
t	time used in integration for given step of loading and/or general time (s)
dt	time increment used in integration for given step of loading (s)
t_c	elapsed time having a fixed origin defined at start of ageing (s)
t_{c1}	time at start of ageing (s)
α^*	parameter of viscosity function (dimensionless)
β	rate sensitivity coefficient (dimensionless)
ε	tensile strain (dimensionless)
ε^{ir}	irreversible tensile strain (dimensionless)
ε_1^{ir}	irreversible tensile strain at start of loading (dimensionless)
$d\varepsilon^{ir}$	irreversible tensile strain increment (dimensionless)
$\dot{\varepsilon}$	tensile strain rate (1/s)
$\dot{\varepsilon}^e$	elastic tensile strain rate (1/s)
$\dot{\varepsilon}^{ir}$	irreversible tensile strain rate (1/s)
$\dot{\varepsilon}_0^{ir}$	parameter of viscosity function (1/s)
τ	irreversible tensile strain used in integration for given step of loading (dimensionless)
$d\tau$	irreversible tensile strain increment used in integration for given step of loading (dimensionless)

ABBREVIATIONS

GRS	geosynthetic-reinforced soil
HDPE	high-density polyethylene
MARV	minimum average roll value
ML	monotonic loading
PET	polyester
PP	polypropylene
SIM	stepped isothermal method
SL	sustained loading
TTS	time-temperature superposition

REFERENCES

- Allen, T. M. & Bathurst, R. J. (1996). Combined allowable strength reduction factor for geosynthetic creep and installation damage. *Geosynthetics International* **3**, No. 3, 407–439.
- ASTM D 4595. *Test Method for Tensile Properties of Geotextiles by the Wide-Width Strip Method*, ASTM International, West Conshohocken, PA.
- Bathurst, R. J. & Cai, Z. (1994). In-isolation cyclic load-extension behavior of two geogrids. *Geosynthetics International* **1**, No. 1, 3–17.
- Bueno, B. S., Costanzi, M. A. & Zornberg, J. G. (2005). Conventional

- and accelerated creep tests on nonwoven needle-punched geotextiles. *Geosynthetics International* **12**, No. 6, 276–287.
- Christopher, B., Bonczkiewicz, C. & Holtz, R. D. (1994). Design, construction and monitoring of full scale test of reinforced soil walls and slopes. In *Recent Case Histories of Permanent Geosynthetic-Reinforced Soil Retaining Walls* (Tatsuoka, F. & Leshchinsky, D. (eds)). Balkema, Rotterdam, pp. 45–60.
- Di Benedetto, H., Sauzéat, C. & Geoffroy, H. (1999). Modelling viscous effects for sand and behaviour in the small strain domain. In *Proceedings of the 2nd International Symposium on Pre-failure Deformation Characteristics of Geomaterials, IS Torino* (Jamiolkowski, M. Lancellotta, R. & Lo Presti, D. (eds)). Balkema, Rotterdam, vol. 2, pp. 1357–1367, panel presentation.
- Di Benedetto, H., Tatsuoka, F. & Ishihara, M. (2002). Time-dependent shear deformation characteristics of sand and their constitutive modelling. *Soils and Foundations* **42**, No. 2, 1–22.
- Di Benedetto, H., Tatsuoka, F., Lo Presti, D., Sauzéat, C. & Geoffroy, H. (2005). Time effects on the behaviour of geomaterials. In *Deformation Characteristics of Geomaterials: Recent Invest and Prospects* (Di Benedetto, H., Doanh, T., Geoffroy, H. & Sauzéat, C. (eds)). Balkema, Rotterdam, pp. 59–123.
- FHWA. (2001). *Mechanically Stabilized Earth Walls and Reinforced Soil Slopes Design and Construction Guidelines*, Federal Highway Administration (FHWA), NHI Course No. 132042, Elias, V., Christopher, B. R. and Berg, R. R., Washington DC, USA, Vol. 73, pp. 114–116.
- Greenwood, J. H., Jones, C. J. F. P. & Tatsuoka, F. (2001). Residual strength and its application to design of reinforced soil in seismic areas. In *Landmarks in Earth Reinforcement, Proceedings of the International Symposium on Earth Reinforcement, IS Kyushu '01*, Fukuoka, Japan (Ochiai, H., Otani, J., Yasufuku, N. & Omine, K. (eds)). Balkema, Rotterdam, vol. 1, pp. 37–42.
- Greenwood, J. H. (2002). The effect of installation damage on the long-term design strength of a reinforcing geosynthetic. *Geosynthetics International* **9**, No. 3, 247–258.
- Hirai, T. & Yatsu, A. (2000). Evaluation method about tensile strength of geogrid to use for dynamic design. In *Proceedings of the 15th Geosynthetics Symposium (Japan Chapter of IGS)*, Tokyo, pp. 205–214 (in Japanese).
- Hirakawa, D., Kongkitkul, W., Tatsuoka, F. & Uchimura, T. (2003). Time-dependent stress–strain behaviour due to viscous properties of geogrid reinforcement. *Geosynthetics International* **10**, No. 6, 176–199.
- Kazmierowicz-Frankowska, K. (2005). Correlation between the results of creep and relaxation tests of geotextiles. *Geosynthetics International* **12**, No. 5, 269–275.
- Kiyota, T. and Tatsuoka, F. (2006). Viscous property of loose sand in triaxial compression, extension and cyclic loading. *Soils and Foundations* **46**, No. 5, 665–684.
- Kongkitkul, W. (2004). *Effects of Material Viscous Properties on the Residual Deformation of Geosynthetic-Reinforced Sand*. PhD thesis, University of Tokyo, 658 pp.
- Kongkitkul, W. & Tatsuoka, F. (2007). A theoretical framework to analyse the behaviour of polymer geosynthetic reinforcement in temperature-accelerated creep tests. *Geosynthetics International* **14**, No. 1, 23–38.
- Kongkitkul, W., Hirakawa, D., Tatsuoka, F. & Uchimura, T. (2004). Viscous deformation of geosynthetic reinforcement under cyclic loading conditions and its model simulation. *Geosynthetics International* **11**, No. 2, 73–99.
- Kongkitkul, W., Hirakawa, D. & Tatsuoka, F. (2007a). Viscous behaviour of geogrids; experiment and simulation. *Soils and Foundations* **47**, No. 2, 265–283.
- Kongkitkul, W., Tatsuoka, F. & Hirakawa, D. (2007b). Rate-dependent load–strain behaviour of geogrid arranged in sand under plane strain compression. *Soils and Foundations* **47**, No. 3, 473–491.
- Koseki, J., Tatsuoka, F., Munaf, Y., Tateyama, M. & Kojima, K. (1998). A modified procedure to evaluate active earth pressure at high seismic loads. *Soils and Foundations*, Special Issue on the Geotechnical Aspects of the January 17, 1995 Hyogoken–Namba Earthquake, 209–216.
- Lee, K., Jones, C. J. F. P., Sullivan, W. R. & Trollinger, W. (1994). Failure and deformation of four reinforced soil walls in eastern Tennessee. *Géotechnique* **44**, No. 3, 397–426.
- Leshchinsky, D. (2001). Design dilemma: use of peak to residual strength of soil. *Geotextiles and Geomembranes* **19**, No. 2, 111–125.
- Liu, H. & Ling, H. I. (2006). Modeling cyclic behavior of geosynthetics using mathematical functions: Masing rule and bounding surface plasticity. *Geosynthetics International* **13**, No. 6, 234–245.
- Shinoda, M. & Bathurst, R. J. (2004). Strain measurement of geogrids using a video-extensometer technique. *Geotechnical Testing Journal* **27**, No. 5, 456–463.
- Shinoda, M., Horii, K., Bathurst, R. J. & Tatsuoka, F. (2002). Investigation of tensile strength after creep and stress relaxation of geogrids. In *Proceeding of the 37th Japan National Conference on Geotechnical Engineering, JGS (Osaka)*, Osaka, pp. 773–774 (in Japanese).
- Tatsuoka, F. (2004). Effects of viscous properties and ageing on the stress–strain behaviour of geomaterials. In *Geomechanics: Testing, Modeling and Simulation, Proceedings of the GI-JGS workshop*, Boston (Yamamuro, J. & Koseki, J. (eds)). ASCE SPT No. 143, pp. 1–60.
- Tatsuoka, F., Koseki, J., Tateyama, M., Munaf, Y. & Horii, N. (1998). Seismic stability against high seismic loads of geosynthetic-reinforced soil retaining structures, Keynote Lecture. In *Proceedings of the 6th International Conference on Geosynthetics*, Atlanta, GA, USA. Industrial Fabrics Association International, St Paul, MN, USA, vol. 1, pp. 103–142.
- Tatsuoka, F., Ishihara, M., Di Benedetto, H. & Kuwano, R. (2002). Time-dependent shear deformation characteristics of geomaterials and their simulation. *Soils and Foundations* **42**, No. 2, 103–129.
- Tatsuoka, F., Di Benedetto, H. & Nishi, T. (2003). A framework for modelling of the time effects on the stress–strain behaviour of geomaterials. In *Proceeding of the 3rd International Symposium on Deformation Characteristics of Geomaterials, IS' Lyon 2003* (Di Benedetto, H., Doanh, T., Geoffroy, H. & Sauzéat, C. (eds)). Balkema, Rotterdam, pp. 1135–1143.
- Tatsuoka, F., Hirakawa, D., Shinoda, M., Kongkitkul, W. & Uchimura, T. (2004). An old but new issue; viscous properties of polymer geosynthetic reinforcement and geosynthetic-reinforced soil structures, Keynote Lecture. In *Proceeding of the 3rd Asian Regional Conference on Geosynthetics (GeoAsia 2004)*, Seoul (Shim, J. B., Yoo, C. & Jeon, H.-Y. (eds)), pp. 29–77.
- Tatsuoka, F., Kongkitkul, W. & Hirakawa, D. (2006). Viscous property and time-dependent degradation of geosynthetic reinforcement. In *Proceeding of the 8th International Conference on Geosynthetics* (Kuwano, J. & Koseki, J. (eds)) Yokohama, Japan, vol. 4, pp. 1587–1590.
- Zornberg, J. G. & Kavazanjian, E. Jr (2002). Closures on: 'Prediction of the performance of a geogrid-reinforced slope founded on solid waste'. *Soils and Foundations* **42**, No. 5, 129–130.
- Zornberg, J. G., Byler, B. R. & Knudsen, J. W. (2004). Creep of geotextiles using time-temperature superposition methods. *ASCE Journal of Geotechnical and Geoenvironmental Engineering* **130**, No. 11, 1158–1168.

The Editor welcomes discussion on all papers published in *Geosynthetics International*. Please email your contribution to discussion@geosynthetics-international.com by 15 February 2008.